PERGAMON

Computers and Structures 76 (2000) 703–712

Computers & Structures

www.elsevier.com/locate/compstruc

On the elastic modulus degradation in continuum damage mechanics

Marcílio Alves[a], Jilin Yu[b], Norman Jones[c,*]

[a]Department of Mechatronics and Mechanical Systems Engineering, University of São Paulo, São Paulo SP 05508-900, Brazil
[b]Department of Modern Mechanics, University of Science and Technology of China Hefei, Anhui 230026, People's Republic of China
[c]Impact Research Centre, Department of Mechanical Engineering, University of Liverpool, Liverpool L69 3GH, UK

Received 2 November 1998; accepted 27 June 1999

Abstract

To measure accurately the elastic modulus of a metal, E, can be a difficult task when a specimen undergoes plastic strains. Moreover, some failure criteria, such as those associated with Continuum Damage Mechanics, require the change of elastic modulus with strain to define a measure of damage, D, in a material or structure. Thus, it is important to assess the possible geometrical influence of a specimen on the measurement of the elastic modulus at different deformation levels. It is shown in this article, with the aid of a numerical simulation, that any plastic strains induce important geometrical effects in the evaluation of E, which have a significant influence on the evaluation of the scalar damage parameter, D.

1. Introduction

Continuum Damage Mechanics (CDM) is sometimes used to predict the phenomenon of failure in structures loaded statically [6,7,12] and dynamically [11,14]. The seminal idea of this method is due to Kachanov [16], who introduced a damage variable, D, to model the phenomenon of creep. Since then, many publications have been produced on this subject and formal theories embracing damage and plasticity [5,13] have been developed.

In the simplest case of isotropic and homogeneous damage, the damage variable, D, is related to the surface density of micro-defects in the material. Clearly, the successful use of CDM to predict failure is related closely to accurate measurements of the damage.

The postulate of strain equivalence, due to Lemaitre [18,19], states that a constitutive equation for a damaged material can be obtained by replacing the stress σ in a virgin material by the effective stress $\tilde{\sigma} = \sigma/(1-D)$, where $\tilde{\sigma}$ is the force divided by the area that effectively sustains the load. Thus, the damage may be represented by an elastic modulus change

$$D = 1 - \frac{\tilde{E}}{E}, \tag{1}$$

where $\tilde{E}$ is the elastic modulus of the damaged material.

Another postulate, known as energy equivalence [8], also relates damage to the change of the elastic modulu but now through the equation

* Corresponding author. Tel.: +44-151-794-4858; fax: +44-151-794-4848.
E-mail address: njones@mechnet.liv.ac.uk (N. Jones).

0045-7949/00/$ - see front matter
PII: S0045-7949(99)00187-X

$$D = 1 - \sqrt{\frac{\tilde{E}}{E}}. \tag{2}$$

Other expressions relating damage to the change in elastic modulus can be found in Luo et al. [22]. Though other techniques can be used to estimate D [1,2,20], it appears that the change in elastic modulus is the most convenient one, both for metals [17,20] and for composites [9,21,26].

Lemaitre and Dufailly [20] and Dufailly [10] were the first researchers to measure D through the degradation of the elastic modulus. A specimen similar to the one depicted in Fig. 1, which is called here a damage specimen, was loaded in tension up to some plastic strain recorded by tiny local strain gauges fixed at the minimum cross-section. The specimen is then unloaded and the elastic modulus is obtained from the slope of the unloading stress-strain curve. After some level of deformation, typically producing strains less than 0.10, the strain gauges fail and are replaced by a new set. The specimen is loaded again to produce further plastic strain and then unloaded to obtain a new value for the elastic modulus. This process is repeated until a visual crack is detected. For ductile metals with failure strains of around one, it is necessary to use at least ten pairs of expensive strain gauges, which require a time-consuming installation.

The test specimens used by Lemaitre and Dufailly [20] and Dufailly [10] had a radius (R_0) of 80 mm which restricts the plastic deformation and, consequently, the damage to a small zone where any changes in the elastic modulus can be monitored. It is acknowledged by Dufailly [10] that this geometry leads to a non-uniform stress field, but it appears that no further attention has been paid in the literature to the influence of this non-uniformity on the measurement of the elastic modulus. Because most of the measurements of D through the elastic modulus degradation are made using similar specimen geometries, it is important to determine whether the measured change in the elastic modulus is due only to material damage or is due partly to specimen geometry effects.

To investigate this aspect, one could test several specimens from the same material with different radii (R_0) and compare the measured elastic moduli at various plastic strains. Alternatively, one could perform a numerical simulation of such a test, investigating possible geometrical effects on the accuracy of the elastic modulus measurement. This last procedure is followed here and it is shown that the initial geometry and the distribution of strains cause an error in the evaluation of the elastic modulus.

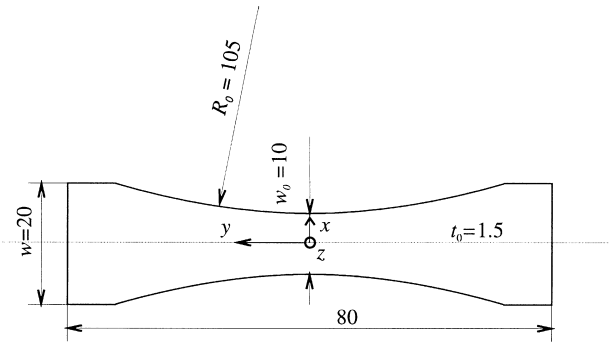

Fig. 1. A typical specimen geometry used to measure the damage parameter D. All dimensions in mm.

2. Method of analysis

The specimen geometry in Fig. 1 was represented by 20 node isoparametric finite-elements with reduced integration type C3D20R, available in the ABAQUS programme. A very fine mesh was used near the smallest cross-section with the initial size of the smallest element being $0.3125 \times 0.05 \times 0.1875$ mm^3 (x,y,z). Thus, a quarter of the cross section includes 64 elements and one-half of a strain gauge with a gauge length of 0.381 mm spans 8 nodes. Advantage was taken of symmetry

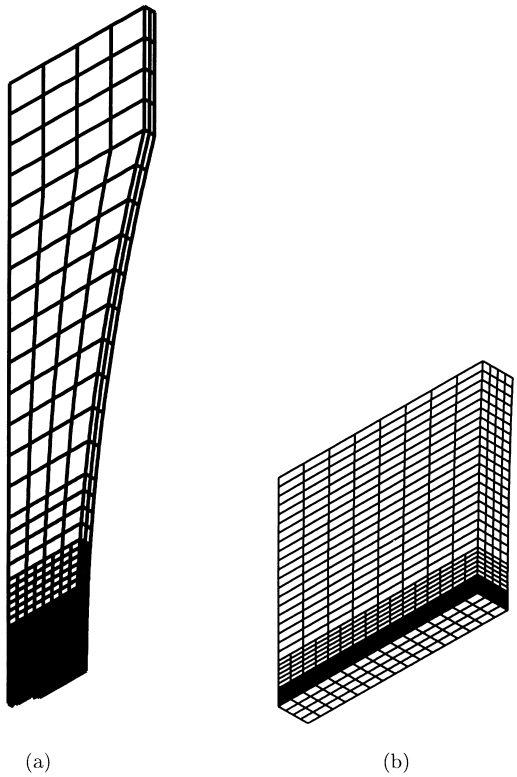

Fig. 2. Finite-element mesh of one-eighth of the damage specimen. (a) Overall mesh and (b) detail of the fine mesh.

to analyse only one-eighth of the specimen, as indicated in Fig. 2.

The incremental theory of plasticity together with the von Mises yield criterion was employed in this study. Material strain hardening was taken as isotropic with no kinematic hardening. Finite deformation or geometrical nonlinearity is considered and the Cauchy stress is used as the true-stress measure. The rate of deformation is used as the strain rate measure,

$$\dot{\varepsilon} = \mathrm{sym}[\partial \boldsymbol{v}/\partial \boldsymbol{x}], \tag{3}$$

where $\boldsymbol{v}$ is the velocity. It is assumed that the total strain rate can be split into elastic and plastic parts. Thus, the change of the total strain during a time step, $\Delta\varepsilon$, can also be divided in two parts, which are calculated according to the corresponding constitutive law.

The total strain measure used in ABAQUS code is the integrated total strain calculated at each time increment as

$$\varepsilon^{n+1} = \Delta \boldsymbol{R} \cdot \varepsilon^{n} \cdot \Delta \boldsymbol{R}^{T} + \Delta\varepsilon, \tag{4}$$

where $\Delta \boldsymbol{R}$ is the incremental rotation tensor. If the principal directions remain fixed in the material axes, then the integrated total strain is equal to the logarithmic strain defined as

$$\varepsilon^{L} = \ln \boldsymbol{V}, \tag{5}$$

where $\boldsymbol{V}$ is the left stretch tensor. Hence, the Cauchy stress and the logarithmic strain curves measured in tensile tests are used as true stress-true strain curves for the numerical simulation. For more details, the reader is referred to the ABAQUS Manual.

The input static equivalent stress–strain curve, shown in Fig. 3, was obtained from a mild steel cylindrical tensile specimen having an elastic modulus and a Poisson's ratio of 209.8 and 0.287 GPa, respectively.

Unlike an experimental test, the present numerical model does not consider any material degradation, i.e. no coupling occurs between plasticity and damage. Thus, the accuracy in evaluating the elastic modulus can be checked more easily. If a comparison is made between the apparent elastic modulus with the actual one measured on the material, or pre-specified in the numerical simulation, then any differences may be safely attributed to geometric effects only.

It is assumed that any damage is isotropic and, hence, that Poisson's ratio in the elastic regime is constant throughout the simulation. This assumption is supported partially by the data in Fig. 4 which was obtained using specimens similar to that shown in Fig. 1 and made of the same material used in this simulation. The apparent constancy of Poisson's ratio in Fig. 4 should be viewed with some reservation since a transverse electro-mechanical extensometer was used to measure the lateral elastic strains. The lateral strains are not constant along x in Fig. 1, so that Poisson's ratio is an average value rather than a local one at $x = 0$, as discussed later.

A linear displacement control function was applied at the top of the specimen. The load path in the simulation consists of nine steps after the initial one, as indicated in Fig. 3. The specimen is loaded up to some level of plastic strain and unloaded until the load is zero. This procedure is repeated in the simulation up to an equivalent strain of 1.02, which is similar to the failure strain for the mild steel here simulated (1.04). Residual stresses generated after unloading have been taken into account in the numerical calculation since any subsequent reloading is applied to the unloaded configuration keeping the calculated residual stresses.

The usual way to calculate the elastic modulus is to measure the applied load, F, the elastic engineering strain, e_e and the current area, A, for each elastic

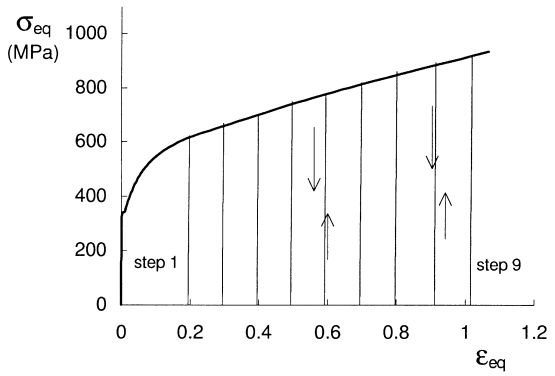

Fig. 3. Static equivalent stress–strain curve for the mild steel used in the simulation. The nearly vertical lines show the various loading–unloading paths applied to the specimen.

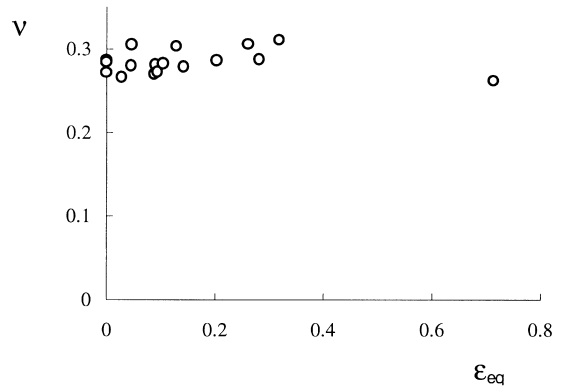

Fig. 4. Evolution of elastic Poisson's ratio with the equivalent plastic strain measured by local axial strain gauges and width contraction of the damage specimens.

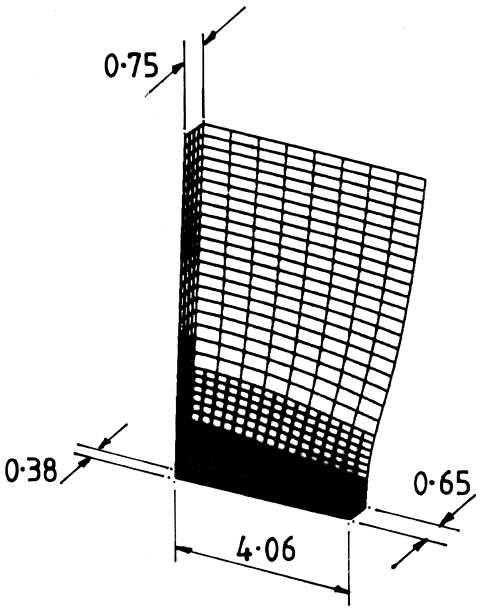

Fig. 5. A detail of the deformed mesh showing the distortion of the mesh in the region of the minimum cross-section of the specimen.

unloading and use the expression

$$E = \frac{F}{Ae_e}. \tag{6}$$

This formula is valid provided the stress field is uniaxial and uniform across the area where the strain gauges are attached. Subsequently, it will be shown that this is not exactly the case in the specimens commonly used in Damage Mechanics since the specimen radius introduces a certain degree of non-uniformity. Moreover, experimental results and the present numerical simulation, do show that the specimen thickness distorts for high plastic strains, as shown in Fig. 5. This suggests even more important non-uniformities in the stress field and, hence, additional errors in the calculation of the elastic modulus if evaluated from Eq. (6). In fact, the elastic modulus given in Eq. (6) is only a material property if the stress and strain fields are uniform otherwise it becomes a geometrically dependent stress–strain ratio which is here called *apparent elastic modulus*, Ξ.

[1] Commercial high elongation small strain gauges have a gauge length of $2 \times 0.1905 = 0.381$ mm.

3. Results

An initial numerical simulation was carried out for the specimen in Fig. 1 but with an infinite radius, i.e. $R_0 = \infty$. This specimen was loaded and unloaded elastically and the output load, area and strain on the external surface were used to calculate the elastic modulus in the usual way. As in a parallel strip with no initial plastic deformation, the stress field is uniform and the calculated elastic modulus must coincide with the input value. This is exactly what was obtained, leading to the conclusion that any value for the elastic modulus different from the input value, in specimens with a lateral radius other than infinity, must be due to geometrical effects only since no damage is considered in the simulation.

Subsequently, the same simulation was performed but with the specimen in Fig. 1, which is called here a damage specimen and three different apparent elastic moduli were obtained.

The first one is obtained using the average value of the elastic strains calculated at the nodes within a length of 0.1905 mm[1] along the central longitudinal axis in the current loaded configuration ($x = 0$, $z = t/2$). That is, during the first loading step, the elastic strains are recorded at these nodes and the final value of the elastic strains is obtained by averaging these elastic strain increments to give an elastic modulus for the first elastic loading simulation $\Xi_s = 214.5$ GPa. As the elastic modulus Ξ_s is different from the input one of $E = 209.8$ GPa it is called here an apparent elastic modulus.

Additionally, two other strain definitions were used to evaluate the elastic modulus. They use the width and change of width (at the middle thickness of the minimum cross-section, $y = z = 0$ in Fig. 1) and thickness and change of thickness (at the middle minimum width, $x = y = 0$ in Fig. 1) to evaluate the elastic contraction strains ε_w and ε_t, respectively. Using these strain definitions, it is possible to define two extra fictitious elastic moduli Ξ_w and Ξ_t, respectively. These strain definitions are easier to obtain than strain gauge data because the width and thickness contractions of a specimen can be measured more easily with an extensometer. Strictly speaking, any change in Poisson's ratio with plastic strain is required in order to obtain the axial elastic strain, which is necessary for the evaluation of the elastic modulus from the width or thickness change. However, as previously stated, the value of Poisson's ratio is assumed to be invariant, Fig. 4. Thus, the elastic moduli using these two strain definitions in the first elastic loading simulation for the damage specimen are $\Xi_w = 221.9$ GPa and $\Xi_t = 208.1$ GPa, again to be compared with $E = 209.8$ GPa.

If further loading–unloading cycles of the specimen

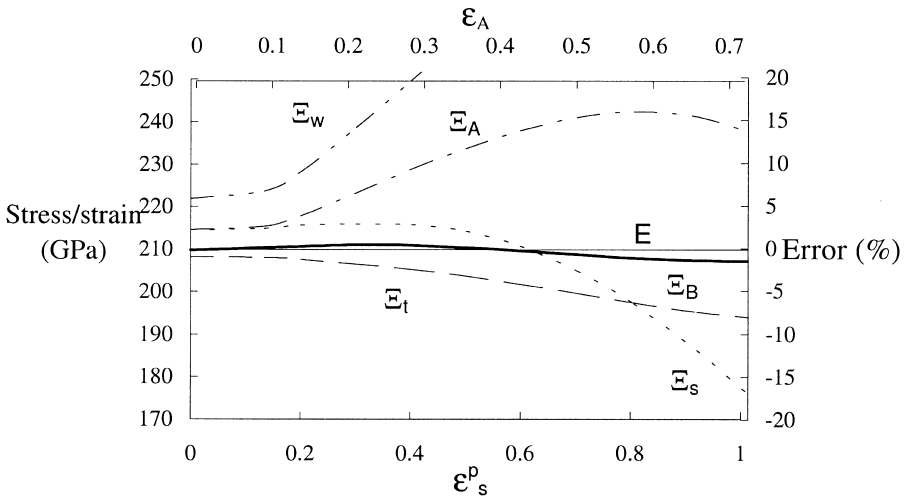

Fig. 6. Change of the apparent elastic moduli, Ξ and associated errors against the actual axial plastic strain ε_s^p and the strain inferred from the area reduction $\varepsilon_A = \ln(A_0/A)$, where A_0 and A are the initial and current areas. Ξ_s, Ξ_t and Ξ_w use the elastic changes in the axial, thickness and width directions, respectively. Ξ_A is evaluated using Eq. (12) and is obtained applying the Bridgman correction factor to Ξ_t.

are conducted at the steps shown in Fig. 3, then Fig. 6 shows the results for the apparent elastic moduli. These are calculated at each step using the current cross-sectional area calculated from the current coordinates of the boundary nodes of the cross-section under the assumption that the line connecting two neighbouring nodes is straight. It is evident that the apparent elastic moduli differ from the material value regardless of the definition of strain. This shows that the technique used to measure E is an important issue if accurate values are sought.

One of the sources of the error in Fig. 6 is due to the non-uniformity of the strain field, as shown in Fig. 7 for the axial elastic strains across the minimum cross-section of the damage specimen. This variation in an actual specimen is more important for the higher plastic strains, when critical damage would occur.

The apparent elastic moduli in Fig. 6 were plotted against the true axial plastic strain, ε_s^p, at $x = 0$ and $z = t/2$ which is averaged over a gauge length of 0.1905 mm[1]. Within this gauge length, the true axial plastic strain along the longitudinal axis of symmetry of the specimen is almost constant for all the steps here considered (Fig. 8). This means that small errors in positioning the strain gauges along this axis are not critical for the evaluation of plastic strains at the minimum cross-section, at least within the range shown in the figure.

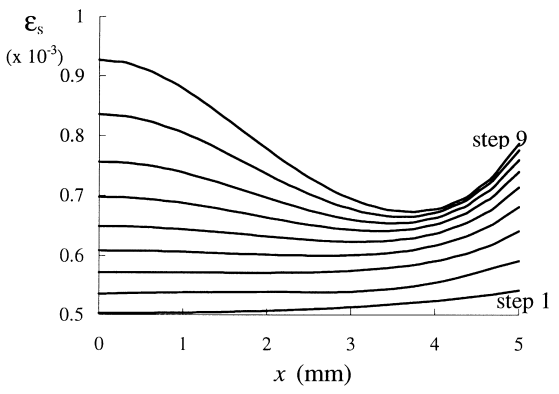

Fig. 7. Numerical results for the elastic axial strains on the surface at the minimum cross-section of the damage specimen ($y = 0$, $z = t/2$) in Fig. 1 at each loading step (referred to the initial configuration).

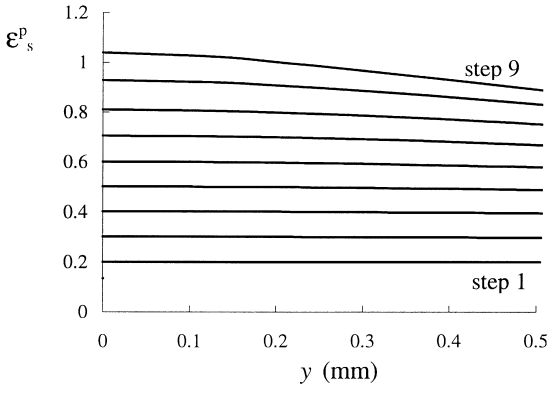

Fig. 8. Numerical results for true axial plastic strain distribution at the various loading steps along the longitudinal axis of symmetry and on the surface of the current configuration ($x = 0$, $z = t/2$).

4. Discussion

It is evident that the specimen geometry in Fig. 1, which is traditionally used to measure the degradation of the elastic modulus, induces non-uniformities in the stress field. Thus, the ratio $F/(Ae_e)$ has a magnitude different from the actual elastic modulus for the material. This non-uniformity is illustrated in Fig. 7; the elastic strains at the middle of a specimen ($x = 0$) are lower than at the boundary ($x = 5$ mm) for the first four steps. This makes the apparent elastic modulus, at those plastic strains, higher than the actual value when strain gauge information from the longitudinal axis of symmetry is used. As the plastic strains increase, the elastic strains at the middle exceed those at the boundary, lowering the apparent elastic modulus.

This strong non-uniformity of the elastic strains make the measurement of them through the width contraction quite unrealistic. In fact, the error in the apparent elastic modulus Ξ_w is unacceptable in Fig. 6, even for small plastic strains.

On the other hand, the contraction in thickness is a good candidate for an easy and relatively accurate technique for measuring the change in elastic modulus since the maximum error is 7.7%, as indicated in Fig. 6. Also, the error evolves in an almost linear fashion in contrast with the strain gauge method. This error can be further reduced to nearly zero when using the Bridgman correction factor, as discussed in the Appendix.

Moreover, the results in Fig. 7 show that within the range $x \pm 1$ mm, the elastic change of the thickness is almost constant, which allows some error in the positioning of a strain sensor.

Other practical reasons also make this method more suitable for the measurement of the elastic modulus. In a typical experiment using strain gauges, a ductile specimen is subjected to around one hundred loading–unloading cycles [24]. At least 20 strain gauges are required and for them to sustain high plastic strains the adhesive needs to be polymerised for several hours in an oven (typically for 3 h). Another difficulty with the use of strain gauges is that the gauge factor changes with the plastic strains [15]. Thus, if strain gauges are used to measure elastic strains after previous plastic deformation, the results must be interpreted with care. The use of an extensometer appears to remove these difficulties without introducing any important problems.

Continuum Damage Mechanics requires not only the damage value, D, but the evolution with deformation. Hence, the importance of measuring accurately the local plastic strains. The use of strain gauges might give acceptable results, but similar information can be obtained from the thickness contraction recorded by an extensometer.

It is assumed that[2]

$$\varepsilon_t^p + \varepsilon_w^p + \varepsilon_s^p = 0 \tag{7}$$

is a good approximation for the damaged material. To calculate an average value for ε_s^p at $x = 0$ and $z = t/2$, here called $\varepsilon_{s'}^p$, the strains ε_t^p and ε_w^p are required, where

$$\varepsilon_t^p = \ln\frac{t_0}{t} \tag{8}$$

and

$$\varepsilon_w^p = \ln\frac{w_0}{w}, \tag{9}$$

so that

$$|\varepsilon_{s'}^p| = \varepsilon_t^p + \varepsilon_w^p. \tag{10}$$

It is evident from Fig. 9 that $\varepsilon_{s'}^p$, as calculated from Eq. (10), is a good estimate of ε_s^p calculated numerically. It follows that the parameters obtained normally from the strain gauge results might be obtained easier and more accurately with an extensometer.

The calculation of the elastic modulus requires the measurement of the current cross-sectional area which is not straightforward since the area distorts as a result of plastic straining, as indicated in Fig. 5. To avoid such difficult measurements, a common practice [10,24] is to estimate the actual area from the expression

$$A = A_0 \exp^{-\varepsilon_s^p}, \tag{11}$$

i.e. the *local* plastic strains measured by the strain gauges are used together with the hypothesis of volume

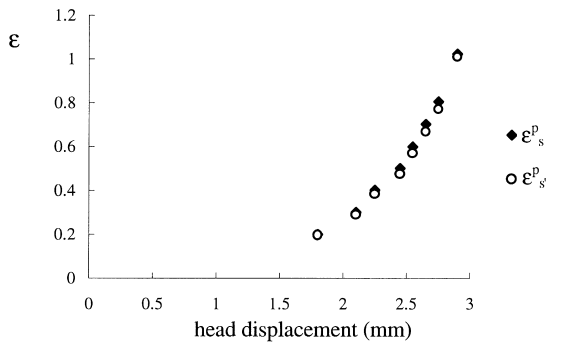

Fig. 9. Comparison between the numerical results for the true axial plastic strain at $x = 0$ and $z = t/2$, as evaluated from the gauge length, ε_s^p and from the thickness and width contraction, $\varepsilon_{s'}^p$, Eq. (10), versus the axial head displacement.

[2] Experimental tests on many metals suggest that the volume of voids present in a damaged material is rather small, which supports this assumption [4,25].

conservation to estimate the current cross-sectional area. Thus, another apparent elastic modulus, Ξ_A, may be defined

$$\Xi_A = \frac{F}{A_0 \exp^{-\varepsilon_s^p} \varepsilon_s}, \tag{12}$$

which has been used by Lemaitre and Dufailly [20] and Dufailly [10]. If the finite-element results are substituted into Eq. (12), then the curve Ξ_A in Fig. 6 is obtained and has a relatively large positive error.

Figure 10 shows the axial plastic strain distribution at the surface ($z = t/2$) across the width of the minimum section ($y = 0$) of the specimen here studied numerically. It is evident that the distribution is not uniform, as observed previously for the elastic strains. This, in turn, introduces an error in the value obtained from Eq. (11).

Now, define the errors in the measurement of the elastic modulus, er_E and of the damage variable obtained from the change of the elastic modulus, er_D, as

$$er_E = \frac{E_i}{E_c} - 1 \tag{13}$$

and

$$er_D = \frac{D_i}{D_c} - 1 \tag{14}$$

respectively (the subscripts i and c stand for incorrect and correct values, respectively). Moreover, the following relations hold:

$$D_i = 1 - \frac{E_i}{E_0} \tag{15}$$

and

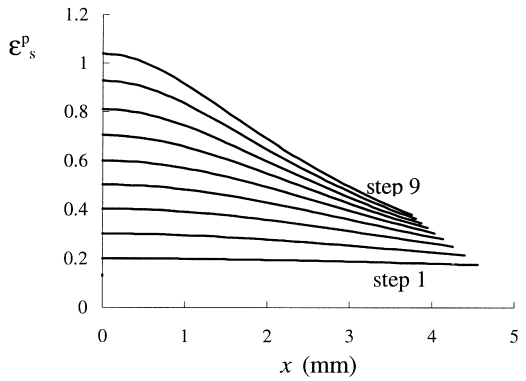

Fig. 10. Numerical value for true axial plastic strain distribution at the various steps along the width at the specimen surface ($z = t/2$) (referred to the current configuration).

$$D_c = 1 - \frac{E_c}{E_0}, \tag{16}$$

where it is assumed that the initial elastic modulus E_0 is correct. By substituting Eqs. (13) and (15) into Eq. (16) and this into Eq. (14) with the notation D_i changed to D_l yields

$$er_D = \frac{er_E(D_l - 1)}{er_E + D_l}, \tag{17}$$

where D_l is the current published damage data inferred from the change in the elastic modulus through Eq. (1). The correct damage value is obtained by substituting Eqs. (13) and (15) into (16)

$$D = D_c = \frac{D_l + er_E}{1 + er_E}. \tag{18}$$

Eqs. (17) and (18) show that if the damage is small the error tends to be quite large. This error is even more important if experimental errors are considered as well as the fact that some published data are based on specimens with radii smaller than the one here analysed. As an example, an error of 10% in the elastic modulus for a damage $D_l = 0.20$ would yield $D_c = 0.27$, an error in D of -26%. This error is reduced to -2% if $D_l = 0.80$, again for $er_E = 10\%$. Here, a negative error indicates that the actual damage is larger than D_l.

It is now possible to plot D and D_l against the plastic strains. To this end, a linear evolution law is selected for the relationship between D_l and the plastic strain ε_s^p at $x = 0$ and $z = t/2$ [18]. This damage behaviour inferred from the change in the elastic modulus is corrected in Fig. 11 according to the error function associated with Ξ_A. It is evident that a large discrepancy occurs for low critical damage values. A similar

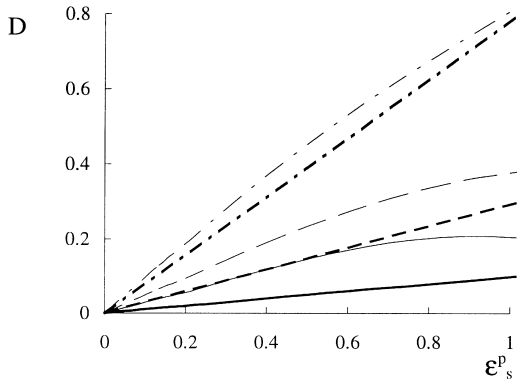

Fig. 11. Evolution of the assumed (thick lines) and corrected (thin lines) damage variable inferred from the change in the elastic modulus versus the actual axial plastic strain at $x = 0$ and $z = t/2$, for critical damage values. —: $D_l = 0.1$, - - -: $D_l = 0.3$ and –·–·–: $D_l = 0.8$. The error function er_E is associated with Ξ_A.

procedure, but now correcting the linear damage evolution using the error curve associated with Ξ_B, is depicted at Fig. 12. The error in this case is reduced by a significant factor, which strongly supports the technique herein proposed.

It should be noted again that the possible actual damage in the specimen and its interaction with plastic deformation are not considered in the current numerical simulation. Hence the influence of damage on the distribution of stress and strain is not taken into account. Further investigation is necessary to evaluate the importance of this effect.

5. Conclusions

Apart from experimental errors, the technique currently used to measure the damage variable, D, through the degradation of the elastic modulus, suffers from some limitations. The specimen geometry is such that it introduces an error even during the first elastic loading due to a nonhomogeneous strain field. This error is not large but it grows as the plastic strains increase.

Different strain measures were defined and used for the evaluation of D. The data gives strong support to the use of an extensometer rather than strain gauges to measure the elastic modulus. Accurate values for E are obtained when using the elastic strains measured during the contraction of the thickness. For the present simulation, such a technique yields a maximum error in the elastic modulus of 7.7%, near the rupture strain.

An error in the evaluation of E has an important effect on the value of the associated damage parameter. This suggests that the current accepted damage values should be corrected by a positive factor, i.e. the actual damage parameter values as defined by $1-\tilde{E}/E$ are larger than the values published in the literature.

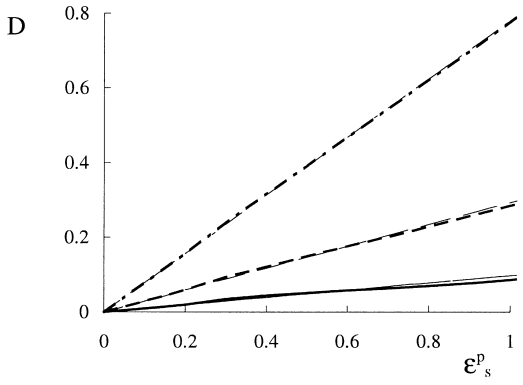

Fig. 12. Evolution of the assumed (thick lines) and corrected (thin lines) damage variable inferred from the change in the elastic modulus versus the actual axial plastic strain for critical damage values. —: $D_l=0.1$, - - -: $D_l=0.3$ and –·–·–: $D_l=0.8$. The error function er_E is associated with Ξ_B.

Acknowledgements

M. Alves was funded by the Brazilian Research Agency, CAPES and the Impact Research Centre and J.L. Yu by the Royal Society, the Chinese Academy of Sciences and the Impact Research Centre. This study forms part of EPSRC grant GR/J 69998 to the Impact Research Centre at the University of Liverpool.

Appendix

Stress triaxiality correction

It is noted in the literature that the damage variable measured by the degradation of the elastic modulus is

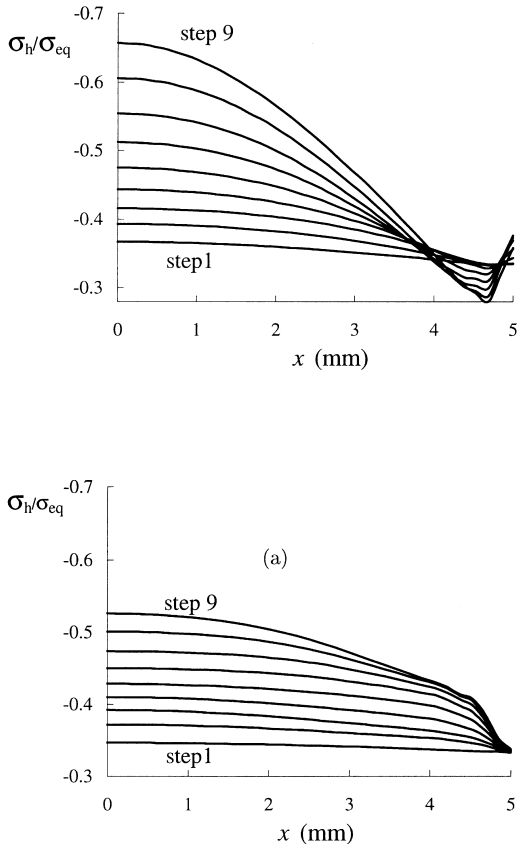

Fig. 13. Numerical prediction for the triaxiality at the (a) middle ($z=0$) and (b) surface ($z=t/2$) of the minimum cross-section ($y=0$) of the damage specimen across the width (referred to the initial configuration).

associated with a uni-dimensional stress field having a hydrostatic to equivalent stress ratio of $\sigma_h/\sigma_{eq}=1/3$. Hence, the published values of the critical damage parameter are considered to be uni-dimensional. Unfortunately, this is not the case for the present specimen geometry and material. Fig. 13 shows the variation of the triaxiality on the middle plane and at the surface of the damage specimen along the width of the minimum cross-section. It turns out that, for large strains, the triaxiality is around twice that for the corresponding uniaxial stress state; a high value typically found in notched cylindrical specimens [23].

Qualitatively, this triaxiality profile resembles the one which occurs in a parallel strip after necking in tension, according to Bridgman [3]. This suggests that a Bridgman correction for the stress field might be applied to the present problem bringing the values of the apparent elastic moduli closer to the actual ones. Moreover, the correction would have the additional advantage of allowing a correlation to be made between damage and stress triaxiality.

To obtain the peak axial stress at the middle of an *infinitely thick* sheet, the average stress F/A is multiplied by [3]

$$f=\frac{1+\ln\left(1+(w/4R)\right)}{\sqrt{1+(4R/w)}\,\ln\left[1+(w/2R)+\sqrt{(w/R)(1+(w/4R))}\right]-1} \tag{A.1}$$

where w and R are the current width and lateral necking radius at the minimum cross-section.

The Bridgman equation is based on an *infinitely wide* sheet and uses the through-thickness necking radius. In the present case, however, necking occurs in both directions but it is more serious on the width (lateral) plane. Thus, instead of using the through-thickness radius, the lateral one on the width plane is used in Eq. (A.1).

It should be noted that, for the specimen in Fig. 1, the stress state and the deformation of the cross-section are more complicated than those in a parallel flat strip. Also, the assumptions in Bridgman's analysis are no longer valid and the method of correction here proposed is essentially approximate. Nevertheless, it is possible that the correction method is reasonable for other specimen materials and geometries since the main factor, i.e. the curvature of the neck, is considered.

The geometrical parameters necessary to apply the correction factor given by Eq. (A.1) may be obtained readily since all the node displacements are available. It is applied to the calculation of the apparent elastic modulus obtained from the thickness contraction Ξ_t. This definition, calculated from equation

$$\Xi_t=\frac{Fv}{A\varepsilon_t}, \tag{A.2}$$

is selected because it is the most accurate in Fig. 6 for large plastic strains.

The ratio F/A is an average value for the axial stress which is multiplied by f, following Bridgman, to obtain another apparent elastic modulus definition

$$\Xi_B=f\frac{Fv}{A\varepsilon_t}=f\frac{\sigma_{\text{ave}}v}{\varepsilon_t}=f\Xi_t. \tag{A.3}$$

This fictitious elastic modulus Ξ_B changes with the axial plastic strain as shown in Fig. 6. Clearly, it yields a better accuracy than the results traditionally obtained via strain gauges.

References

[1] Asundi A. Damage measurement in aluminium using the Moiré method. In: Jono M, Inoue T, editors. Mechanical behaviour of materials, VI. Pergamon Press, 1991. pp. 823–8.

[2] Bourban P, Cantwell W, Kausch H, Youd S. Damage initiation and development in chopped strand mat composites. In: Miravete A, editor. Composites behaviour. University of Zaragoza and Woodhead Publishing Ltd, 1993. pp. 79–86.

[3] Bridgman P. Studies in large plastic flow and fracture. New York: McGraw-Hill, 1952.

[4] Brownrigg A, Spitzig W, Richmond O, Teirlinck D. The influence of hydrostatic pressure on the flow stress and ductility on a spherodized 1045 steel. Acta Metallurgica 1983;31(8):1141–50.

[5] Carol I, Rizzi E, Willam K. A unified theory of elastic degradation and damage based on a loading surface. International Journal of Solids and Structures 1994;31(20):2835–65.

[6] Cipollina A, López-Inojosa A, F1órez-López J. A simplified damage mechanics approach to nonlinear analysis of frames. Computers & Structures 1995;54(6):1113–26.

[7] Combescure A, Jiaju Y. Finite element method for large displacement and large strain elasto-plastic analysis of shell structures and some application of damage mechanics. Engineering Fracture Mechanics 1990;36(2):219–31.

[8] Cordebois J, Sidoroff F. Damage induced elastic anisotropy. In: Boehler J, editor. Mechanical behaviour of anisotropic solids. London; Paris: Martinus Nijhoff Publishers; Editions du CNRS, 1979. pp. 761–74.

[9] Delaet M, Lataillade J, Wolff C. Intralaminar shear loading effects on the damage process of multiply composites at impact rates. In: International Conference on Mechanical and Physical Behaviour of Materials under Dynamic Loading - Journal de Physique IV. Les Éditions de Physique and DYMAT, 1994. pp. 213–8.

[10] Dufailly J. Modelisation mecanique et identification de l'endomagement plastique des metaux. Ph.D. thesis,

Laboratoire de Mecanique et Technologie, Universite P.M. Curie. Cachan, France, 1980.

[11] Faruque M, Wu H. Damage mechanics based constitutive model: application in crash analysis of aluminium components. In: Ju J, Valanis K, editors. Damage Mechanics and Localization, Volume AMD-142. ASME, 1992. pp. 41–52.

[12] Ghrib F, Tinawi R. Nonlinear behaviour of concrete dams using damage mechanics. Transactions of the ICE — Journal of Engineering Mechanics 1995;121(4):513–27.

[13] Hansen N, Schreyer H. A thermodynamically consistent framework for theories of elastoplasticity coupled with damage. International Journal of Solids and Structures 1994;31(3):359–89.

[14] Haug E, de Rouvray A. Crash response of composite structures. In: Jones N, Wierzbicki T, editors. Structural crashworthiness and failure. Barking, Essex: Elsevier Science Publishers, 1993. pp. 237–94.

[15] Huang S, Khan A. On the use of electrical-resistance metallic foil strain gages for measuring large dynamic plastic deformation. Proceedings of the Society for Experimental Mechanics 1991;XLVIII:122–5.

[16] Kachanov L. Time of the rupture process under creep conditions. Ivz Akad Nauk SSR Otd Tech Nauk 1958;8:26–31.

[17] Kim S, Kim W. A progressive damage modeling based on the continuum damage mechanics and its finite element analysis. Journal of Applied Mechanics 1994;61:45–53.

[18] Lemaitre J. A continuous damage mechanics model for ductile fracture. Journal of Engineering Materials and Technology 1985;107:83–89.

[19] Lemaitre J. A Course on Damage Mechanics. Berlin and New York: Springer Verlag, 1992.

[20] Lemaitre J, Dufailly J. Damage measurements. Engineering Fracture Mechanics 1987;28(5/6):643–61.

[21] Lemaitre J, Leckie F, Sherman D. Crazing of laminates. European Journal of Mechanics, A/Solids 1992;11(3):289–304.

[22] Luo A, Mou Y, Han R. A large anisotropic damage theory based on an incremental complementary energy equivalence model. International Journal of Fracture 1995;70:19–34.

[23] Mackenzie A, Hancock J, Brown D. On the influence of state of stress on ductile failure initiation in high strength steels. Engineering Fracture Mechanics 1977;9:167–88.

[24] Nouailhas D. Etude experimentale de l'endomagement de plasticite ductile anisotrope. Ph.D. thesis, Laboratoire de Mecanique et Technologle, Universite P.M. Curie. Cachan, France, 1980.

[25] Shi Y, Barnby J, Nadkarni A. Void growth at ductile crack initiation of a structural steel. Engineering Fracture Mechanics 1991;39(1):37–44.

[26] Tang C, Plumtree A. Damage mechanics applied to polymers. Engineering Fracture Mechanics 1994;49(4):499–508.